Decay of hollow atoms in Ne^{10+}-C_{60} collisions

S. Martin,[1] L. Chen,[1] R. Brédy,[1,*] J. Bernard,[1] A. Salmoun,[1,2] and B. Wei[3]
[1]*Laboratorie de Spectrométrie lonique et Moléculaire, Université Lyon 1, UMR CNRS 5579, Campus de la Doua, 69622 Villeurbanne Cedex, France*
[2]*Faculté des Sciences Semlalia, Université Cadi Ayyad, Boîte Postale 2390, Marrakech, Morocco*
[3]*Institute of Modern Physics, Chinese Academy of Sciences, Lanzhou 730000, China*
(Received 16 July 2003; published 14 April 2004)

We have studied the decay of hollow atoms formed in Ne^{10+}-C_{60} collisions at low energy ($E=100$ keV). The decay products of hollow atoms, i.e., the scattered projectiles and the number of ejected electrons from autoionization cascades, have been measured. The projectile energy loss has been analyzed as a function of the final charge state, in order to differentiate collisions at large distance, near the C_{60} through the electronic clouds and inside the C_{60} cage. For scattered projectiles Ne^{8+} where two electrons are stabilized ($s=2$), up to 16 ejected electrons have been observed, and lower energy loss compared to projectiles with more stabilized electrons ($s>2$) has been measured. These results are interpreted by the formation and relaxation of completely neutralized compact hollow atoms passing very close to the C_{60} molecule (into the electron clouds). The observed large number of ejected electrons is explained by a direct filling of the *N* shell during the interaction time and a fast decay via quasicomplete autoionization cascades.

DOI: 10.1103/PhysRevA.69.043202 PACS number(s): 36.40.−c, 34.50.−s

I. INTRODUCTION

The formation and relaxation of hollow atoms have been studied intensively in recent years. Most of the theoretical and experimental works have been performed to investigate hollow atoms formed during the interaction of highly charged ions with a metallic or insulator surface at different incidence angles [1–7]. Alternative experiments have been carried out using a thin metal foil target with straight microcapillaries [8]. A large fraction of transmitted projectiles having stabilized only a few electrons have been observed, and free hollow atoms have been studied in vacuum by x-ray spectroscopy. More recently, collisions between slow highly charged ions (SHCI) and clusters, in particular the C_{60} molecule, have been investigated experimentally and theoretically [9–15]. Several types of interactions have been analyzed and defined as atomlike, surfacelike, and solidlike interactions, depending on the impact parameters.

In collisions between SHCI and solid, surface, microcapillary, or cluster targets, a common scenario, called "above and below the target," has therefore emerged. As the SHCI approaches the target, it becomes neutralized at a critical distance by resonant electron transfer as described in a classical over barrier model (CBM), leading to the above-target formation of the so-called hollow atoms of the first generation (HA1). The Auger rates of HA1 have been found to be rather small in the cases of SHCI-surface interactions due to a broad population distribution on the electronic *n* levels. The structure of multiply excited atoms with many inner-shell vacancies depends strongly on the binding energy of each captured electron on the target and on the estimation of the dynamic screening during the electron transfer process. As a result, the HA1 obtained with a "metallic" clusterlike C_{60} also has a broad electronic *n*-level distribution [1,9]. Then the stabilization process by Auger decay during the SHCI-C_{60} interaction time does not start efficiently. As the projectile penetrates the target below the surface or inside the cluster, the ion charge is dynamically screened by the valence electrons of the target, leading to a promotion of the energy levels. Resonant charge transfer can occur on the inner shells and a more compact hollow atom of the second generation (HA2) can survive temporarily with Auger rates much higher than in the HA1. This mechanism allows us to interpret the very fast neutralization of highly charged ions in SHCI-carbon foil collisions [16].

Compared to SHCI-surface or -solid collisions, the SHCI-cluster collisions present some advantages because of the limited dimension of the target. In atomlike collisions at large impact parameters, the HA1 decays after the interaction time, out of target perturbation. Coincidence measurements of the projectile final charge state and the number of ejected electrons have enabled us to get precise information on the autoionization cascades of free hollow atoms [17]. The solidlike collisions are characterized by the energy loss of the projectile. Direct evidence of the fast Auger decay of the HA2 has been provided in Xe^{30+}-C_{60} frontal collisions where a number of ejected electrons has been measured larger than the initial projectile charge (about 60). In surfacelike interactions, i.e., in collisions with intermediate impact parameters without projectile energy loss, a number of ejected electrons larger than the initial charge of the projectile have been observed [18]. The last phenomenon has also been observed with an O^{8+} projectile. However, using projectiles of the same charge with lower potential energy Ar^{8+}, no fast electron ejection, neither in frontal collisions nor in surfacelike collisions, has been observed at all. It strongly suggests that the fast electron ejection near the C_{60} depends sensibly on the nature of the projectile and not only on its initial charge.

*Present address: James R. Macdonald Laboratory, Department of Physics, Kansas State University, Manhattan, KS 66506-2604, USA.

Thus this fast electron ejection cannot be interpreted using a simple projectile charge-C_{60} interaction model which, for example, leads to electron loss from the target due to electron recapture. To interpret such an observation, we introduce in the present work the notion of the formation of a more compact hollow atom of the first generation (CHA1) near the target described as follows. In A^{q+}-C_{60} collisions, the HA1 is formed as far as the collision distance is larger than R_q, the critical distance for the projectile neutralization. The CBM predicts that the capture level of electrons ranges from n_1 to n_q ($n_q < n_1$) for the first and the q^{th} captured electron. Under this critical distance, the electrons already in highly excited states return to empty shells of the target and a large number of electrons are transferred quasisimultaneously to the projectile on the same inner shell, n_q, leading to the formation of the compact hollow atom of the first generation (CHA1). The lifetime of such hollow atoms is estimated to be much shorter than the collision time [14]. Therefore, the fast decay of the CHA1 during the collision time and the continuous electron supply from the target to the CHA1 allows us to interpret the large number of electrons ejected in surfacelike collisions. It frontal collisions, the formation of the CHA1 corresponds to a transitory step in the evolution of the HA1 formed at large distance and the HA2 inside the cluster target.

In this paper, we report an experimental investigation of collisions between bare Ne^{10+} ions and C_{60}. We have measured the partial cross sections σ_r^s, where s is the number of electrons stabilized on the projectile and r, called the active electron number, is the number of electrons lost by the C_{60}. Short and long distance collisions are separated by energy-loss analyses for different final charge states of the scattered projectiles. In the special case where two electrons are stabilized on the projectile ($s=2$), we tentatively interpret the measured number of ejected electrons using the dynamical picture of the formation and fast decay of a CHA1 on the N-shell. For collisions at long distances, a statistical model, developed initially by Russek and Meli [19], has been used to estimate the average number of ejected electrons.

II. EXPERIMENTAL TECHNIQUE

The experimental setup has already been described [20], and only the main features and recent modifications are presented. The $Ne_{22}{}^{10+}$ ion beam was extracted with a voltage of 10 kV from the ECR source at GANIL (LIMBE) in Caen. To ensure a good parallelism, the ion beam was aligned and collimated using an entrance slit followed by two holes 500 μm in diameter. The collision region was defined by the perpendicular crossing between the ion beam and an effusive C_{60} gas jet. In this experiment, the neutral C_{60} beam was along the horizontal axis, whereas in our previous experiments the C_{60} jet was along the vertical axis. Ejected electrons and recoil ions were extracted towards opposite sides of the collision region by an electric field of 800 V/cm. The $Ca_{60}{}^{r+}$ ions or charged fragments were analyzed using a time-of-flight (TOF) tube 30 cm in length situated above the extraction plates along the vertical axis. The recoil ions are detected with two multichannel plates (MCP) followed by a multianode of 121 pixels. The collection and detection efficiencies have been measured to about 75 % for multicharged $C_{60}{}^{r+}$ ($r=2-6$) ions and light monocharged fragments from asymmetrical fission. The detection efficiency for monocharged C_{60} ions (50 %) is found to be lower than the monocharged light fragments. The background vacuum has been improved by two orders of magnitude to reach 1.2×10^{-9} mbar with the oven in operation. The electrons were focused, accelerated at 20 keV, and sent toward a semiconductor detector (PIPS). The number of ejected electrons in a single coincidence event was determined by measuring the total energy deposited by all collected electrons in the detector. The electron spectrum has to be corrected for backscattered electron effect using the standard methods described in Ref. [20]. From triple coincidence measurements of an intact multicharged C_{60} ion, the number of electrons, and the final charge state of the projectile, the electron collection efficiency has been estimated to be 0.86 [20]. The outgoing projectile was analyzed in charge state and in kinetic energy by a 90° electrostatic cylindrical analyzer ($R=150$ mm) situated in the horizontal plane with an energy resolution of 1/200 and an acceptance angle of ±2.8°. A channeltron electron multiplier (CEM) detected the projectile ions with detection efficiency close to 100 % at the applied energy range. The principle of the measurements of σ_r^s cross sections and kinetic energy of a scattered projectile has been precisely explained in Ref. [20].

III. EXPERIMENTAL RESULT AND DISCUSSION

Measurements have been performed in event-by-event list mode, recording in coincidence the electrostatic analyzer voltage, the amplitude of the electron signal, the number of recoil ions hitting the "multianode" detector, and the time of flight of each fragmented or intact $C_{60}{}^{r+}$ recoil ion. From the event files, several two-dimensional (2D) spectra can be sorted out. The projectile-recoil ion (PR-RI) spectrum is a 2D histogram in which the horizontal axis stands for the TOF of the heaviest fragment recoil ion of an event and the vertical axis for the scanning of the electrostatic analyzer voltage. In Fig. 1(a), we present a typical PR-RI spectrum obtained for a scan around the peak of scattered projectiles $Ne^{(10-2)+}$ ($s=2$). The kinetic energy spectrum of the scattered projectiles Ne^{8+} can be obtained by the vertical projection of this 2D spectrum. In order to emphasize the contribution of the population with an energy loss, in Fig. 1(b) we show only the partial vertical projection associated to light fragments C^+, $C_2{}^+$ and $C_3{}^+$. The experimental data [Fig. 1(b)] are fitted by two Gaussian peaks. The peak at lower analyzer voltage corresponds to projectiles with lower kinetic energy with respect to the peak at higher analyzer voltage. They are attributed to collisions at small impact parameters and at large parameters, called IN and OUT components, respectively. The energy loss of the OUT component is found to be lower than 100 eV with the absolute calibration of the electrostatic analyzer. It is neglected in the following. From the gap between the two components, we have estimated an energy loss of 490 eV for collisions at short distances in the case of $s=2$.

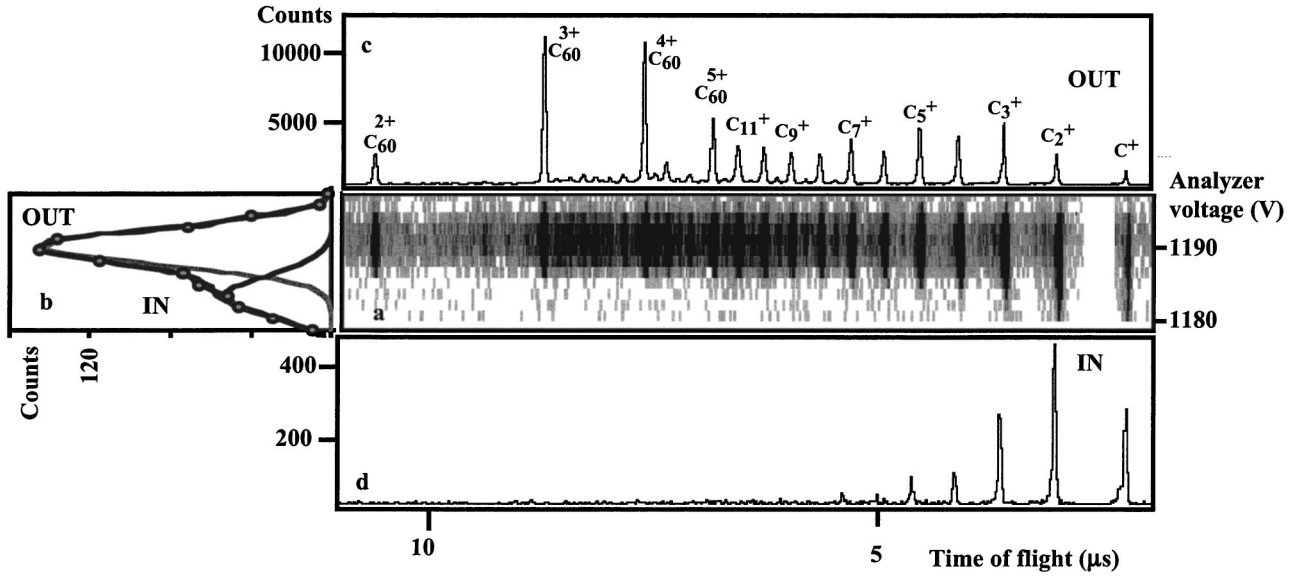

FIG. 1. (a) 2D spectrum in Ne^{10+}-C_{60} collisions. The horizontal axis stands for the TOF of the heaviest fragment recoil ion of an event and the vertical axis for the scanning of the electrostatic analyzer voltage around the Ne^{8+} peak. (b) Partial vertical projection for C^+, C^{2+}, and C^{3+} ions. The broad peak is the summation of two peaks (IN and OUT components) of Gaussian shape. The "zero" energy loss corresponds to the OUT component. (c) and (d) Partial horizontal projections for OUT and IN contributions, taking into account the two components of (b).

The energy losses measured for scattered projectiles with the final charge state ranging from 5 to 8 are presented in Fig. 2 versus the stabilized electron number s with a typical error bar of about ±100 eV. An average energy loss of about 600 eV is obtained. Using the SRIM program [21], the electronic and nuclear stopping powers of Ne at $v=0.42$ a.u. in a carbon solid target are found to be 430 and 170 eV/nm, respectively. In the case of a C_{60} target, using nonadiabatic quantum molecular-dynamics calculations, Kunert *et al.* [22] have shown that at the present projectile velocity range, the nuclear contribution is much smaller than the one estimated in the SRIM calculations. Considering an effective thickness of a C_{60} target as 0.5 nm and neglecting the nuclear energy loss, we obtain a calculated energy loss of about 215 eV, which is much smaller than the measured value ($\Delta E \simeq 600$ eV). This latter high value of energy loss is due to the strong preequilibrium effect when the mean projectile charge during the collision is higher than the equilibrium charge of the projectile in the target [$q_{eq}=Z^{1/3}v$; Z,v (a.u.) are the atomic number and the velocity of the target] [23]. In our previous $Xe^{q+}-C_{60}$ ($q=8-30$) collision experiments, a quadratic energy-loss dependence on the initial projectile charge q was observed [24].

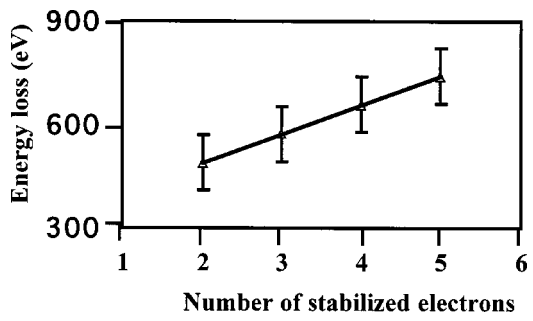

FIG. 2. Energy loss vs number s of stabilized electrons on the projectile.

In the case of Ne^{10+}-C_{60} collisions, the mean charge of the projectile during the collision can be estimated roughly by measuring the final charge of the scattered ions $Ne^{(10-s)+}$. The energy loss is expected to increase as the difference between the final charge state of the scattered projectiles and the equilibrium charge increases. Consequently, if the energy-loss variation is only due to a projectile charge effect, the energy loss should be enhanced for smaller values of s. However, in our experiment, the opposite variation tendency has been observed. The linear increase from 490 to 740 eV for s varying from 2 to 5 (Fig. 2) should then be considered as the signature of another effect. As shown in [11] (Fig. 9) and [22] (Fig. 4), the energy loss is found to be lower in collisions with impact parameters in the range of 7–9 a.u. than those through the C_{60} cage near the center. We then associate different energy loss to collisions with different projectile trajectories through or near the C_{60} cage. For the case of $Ne^{(10-2)+}$ ($s=2$), the IN component which has the lowest measured energy loss could be attributed to collisions where the projectiles pass close to the surface of the C_{60} cage and inside the electronic clouds.

For collisions with the same projectile final charge state, TOF spectra associated with collisions at large and small impact parameters can be obtained. In the case of $s=2$, horizontal projection of the upper part of the 2D spectrum [Fig. 1(a)] including the intact $C_{60}{}^{r+}$ ($r=2-5$) ions is obtained [Fig. 1(c)]. This part of the spectrum corresponds mainly to collisions at large impact parameters without energy loss and is associated with the OUT component in Fig. 1(b). It is composed of intact $C_{60}{}^{r+}$ ions and monocharged $C_n{}^+$ fragments (from $C_1{}^+$ to $C_{14}{}^+$). The horizontal projection of the

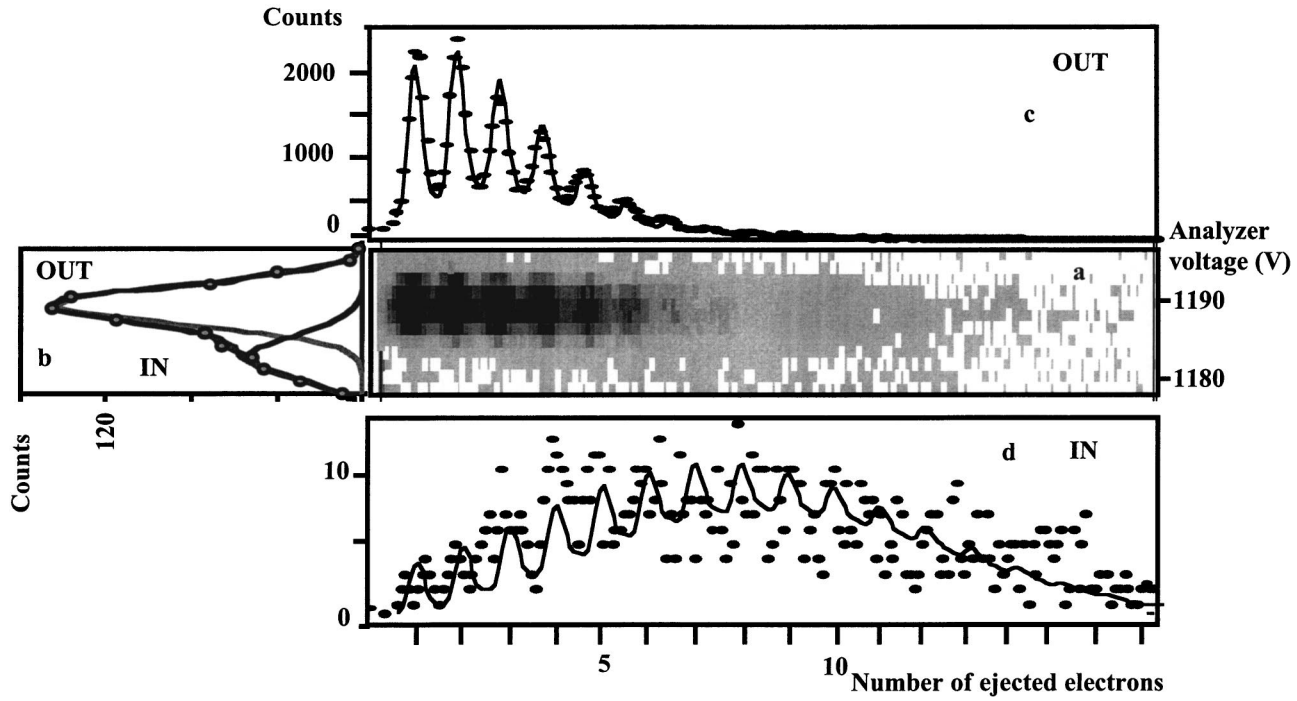

FIG. 3. (a) Coincidence between the Ne^{8+} ($s=2$) outgoing projectile and the amplitude of the electron signal corresponding to the number of ejected electrons. (b) Partial vertical projection, only contribution of C^+, C_2^+, and C_3^+ fragments. (c) and (d) Partial horizontal projection for OUT and IN contributions. The "zero" electron peak is recorded in the channel zero and has been removed from the figure to clarify it.

lower part of the 2D spectrum [Fig. 1] shown in Fig. 1 is associated mainly with the IN component of the projectile. In strong contrast to the spectrum (c), only light C_n^+ fragments (from C_1^+ to C_5^+) are observed. In fact, the real partial population distribution of the light fragments is obtained by recording the PR-RI multistop spectrum (not shown here), in which all charged fragments are recorded for each event. The dominant peak in the multistop TOF IN spectrum is the C^+ ions.

The correlation between the projectile energy loss and the ejected electron number is shown in two-dimensional projectile-electron (PR-EL) spectra [Fig. 3(a)], in which the horizontal axis stands for the amplitude of the electron signal and the vertical axis for the analyzer scanning voltage. The PR-EL spectra have been recorded for a different final charge state of the projectile $Ne^{(10-s)+}$ with s ranging from 1 to 6. In Fig. 3(b), we present a typical PR-EL spectrum for $Ne^{(10-2)+}$ outgoing projectiles ($s=2$). Figure 3(b) is the vertical projection of this spectrum obtained with an extra criterion for the detection of the light fragments C^+, C_2^+, and C_3^+ in order to emphasize the contribution of the IN component. Partial horizontal projections of the upper and lower parts of the 2D spectrum associated with the projectile OUT and IN components are presented in Figs. 3(c) and 3(d), respectively. The mean electron numbers are found to be around $\langle n\rangle=3$ for the OUT component and $\langle n\rangle=8$ for the IN component. It is noteworthy that the distribution of the number of ejected electrons for the IN component extends up to $n=16$, leading to 18 active electrons ($r=n+2$). Therefore, we can deduce that in grazing collisions characterized by $s=2$ and an energy loss of about 490 eV, at least 8 (18−10) electrons should be ejected during the interaction time in accordance with our assumption of the formation and fast relaxation of the CHA1 in "above surface" collisions.

From the partial electron number distribution spectra ($s=1-6$) related to the IN and OUT components, we have measured the σ_r^s cross sections (Fig. 4). The electron number conservation rule $r=n+s$ is used to calculate the number r of active electrons. The total cross section $\sigma=\Sigma_{r,s}\sigma_r^s$ is normalized to the value $\sigma=2700$ a.u. corresponding to the cross section πR_1^2 for the capture of the first electron in Ne^{10+}-C_{60} collisions using the CBM. The critical distance R_1 has been found to be 29.6 a.u. [15] and 29 a.u. (Fig. 4 in [12]), respectively. For the largest s value ($s=6$) related to inside C_{60} cage collisions, up to 27 active electrons are measured, providing clear evidence that the active electron number r

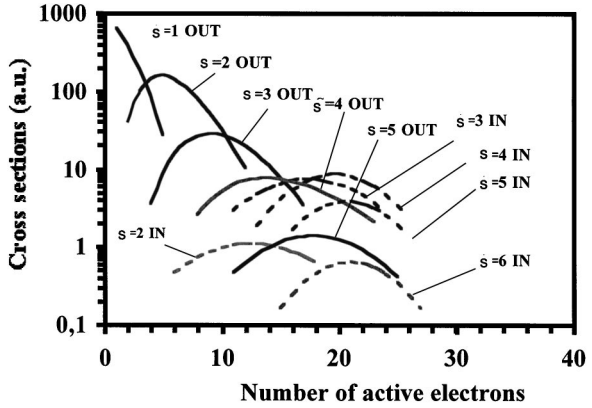

FIG. 4. Cross sections σ_r^s vs the number r of active electrons for OUT and IN collisions. Each curve is related to a selected final charge state of the projectile and so for a given number s.

exceeds largely the projectile initial charge. A similar effect has been observed in Xe^{30+}-C_{60} collisions [15]. In the above two cases, the maximum number of active electrons is about three times the projectile initial charge. However, in Ar^{8+}-C_{60} frontal collisions, despite the fact that the charge of the projectile is closer to the Ne^{10+} case, the maximum active electron number has been found to be much smaller (around 8). Furthermore, in Ne^{10+}-C_{60} experiments, the collection probability of ejected electrons was found to be about 0.86, which is lower than the one found in the Ar^{8+} case (0,92). These observations can be interpreted by the important difference of the potential energies of the two projectiles (3 and 5 keV for Ne^{10+}, 0 and 57 keV for Ar^{8+}). Indeed, the potential well of a hollow atom with a bare ion Ne^{10+} is much deeper than the potential well with an atomic core like Ar^{8+}, for which the *K* and *L* shells are filled. Therefore, the autoionization cascade follows a greater number of steps for hollow atoms with a bare ion like Ne^{10+}, leading to a larger number of ejected electrons. Furthermore, higher average kinetic energy of autoionized electrons is expected in the Ne^{10+} case, especially at the last steps of autoionization cascades to fill the *K* shell ($E \sim 1.3$ keV for 1*s* state). The relation between the electron collection efficiency and the kinetic energy of the electrons has been demonstrated in our previous experiment [25].

Figure 4 shows that the mean number of active electrons is about 12 and 22 in the cases of $s=2$ and 6 IN collisions, respectively (Fig. 4). Therefore, 12 and 22 light charged fragments (mainly C^+) should be expected due to the multifragmentation of $C_{60}{}^{12+}$ and $C_{60}{}^{22+}$ parent ions. However, the mean number of detected charged fragments per event is measured to be only about five in the case of $s=2$ and seven in the case of $s=6$. The effective collection and detection efficiency of each fragment is then estimated to be about 0.4 and 0.3 for the multifragmentation of $C_{60}{}^{12+}$ and $C_{60}{}^{22+}$, respectively. These numbers are much smaller than the detection efficiency (0.75) of our TOF spectrometer. It should be due first to the complete Coulomb explosion of the multiply charged C_{60} leading to fragments with high kinetic energy and therefore lower collection efficiency, and second to the strong probability that two C^+ fragments are considered as only one fragment when they hit the same anode pixel quasisimultaneously.

The σ^s cross sections as a function of the stabilized electron number s for IN and OUT components (Fig. 5) are obtained from the measured partial σ_r^s cross sections by the relation $\sigma^s = \Sigma_r \sigma_r^s$. The total cross section for IN collisions is found to be 225 a.u. It is in fairly good agreement with the geometrical cross section of the C_{60} including the electronic cloud which is 283 a.u. ($R_o \sim 9.5$ a.u.). The *s* dependence of the average number of ejected electrons $\langle n \rangle$ is shown in Fig. 6 for the IN and OUT collisions, respectively. The linear dependence of $\langle n \rangle$ versus *s* for the OUT component means that a constant number of electrons ($\approx 2,5$) are ejected for HA1 to stabilize one more electron. Due to the electron distribution on a large number of n shells, the relaxation of HA1 occurs after the collision via radiative transitions as well as autoionizing cascades. The evolution of HA1 with a number of active electrons up to 10 has been investigated using a

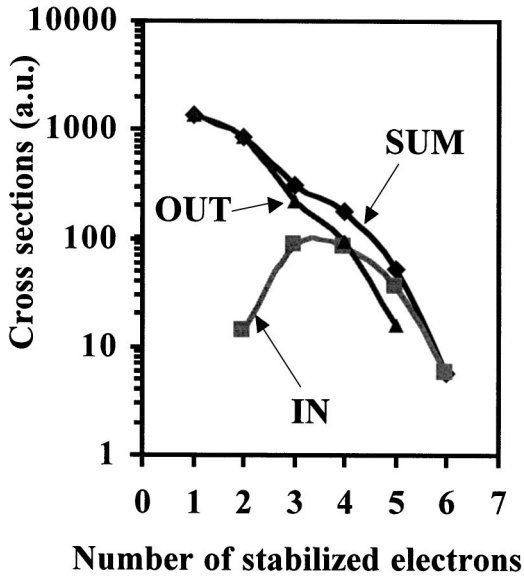

FIG. 5. Cross sections σ^s vs the number *s* of stabilized electrons for OUT ($s=1-5$) and IN ($s=2-6$) contributions.

statistical model. The Russek and Meli [19] model has been employed to reproduce the measured cross sections by adjusting a *g*-factor parameter. The parameter g^n is proportional to the mean-square matrix elements of transitions from initial states with *r* active electrons to all possible final states in which n electrons are ejected. The details of this model applied to the autoionization of HA1 will be given in a forthcoming paper [26]. Figure 7 shows the measured and calculated mean number of ejected electrons $\langle n \rangle$ versus the number r of active electrons. The agreement between experimental and theoretical values is fairly good using an adjusted value of 0.9 for the *g* factor.

In strong contrast, for "IN" collisions more ejected electrons are observed and the *s* dependence of $\langle n \rangle$ shows a saturation effect for larger *s* value. For $s=2$ and 3, about seven more electrons are ejected in "IN" collisions than in "OUT" collisions (Fig. 6). This difference can be qualitatively understood by the formation of CHA1 and HA2 at short impact parameters. The fast Auger decay of compact hollow atoms during the collision time allows us to interpret the large number of ejected electrons. The saturation effect

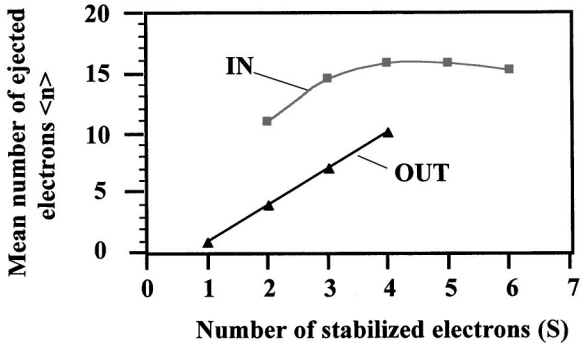

FIG. 6. Mean number of ejected electrons $\langle n \rangle$ versus the number *s* of stabilized electrons for the IN and OUT components, respectively.

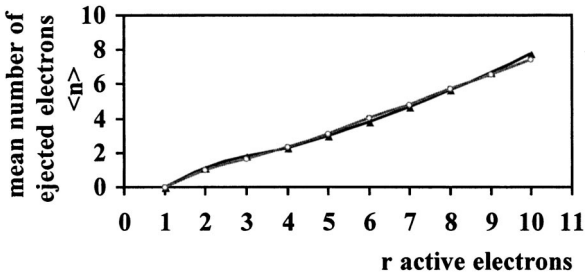

FIG. 7. Mean number of ejected electrons $\langle n \rangle$ versus the number of active electrons. ○, experimental data; ▲, theoretical values obtained with the statistical model.

observed for $s=4,5,6$ is probably due to the formation of HA2 inside the C_{60} cage where the electrons are transferred to inner-shell vacancies ($n<4$) of Ne^{10+}. The relaxation of such HA2 with electron population of lower levels needs a few steps in autoionization cascades.

Now let us consider the special case $s=2$ and focus our attention on the results for IN collisions. The cross section of these events presents about 5 % of the total IN cross sections. This value is comparable to the relative cross section of the ring of electronic clouds outside the C_{60} cage. It gives another argument for our attribution of these events to the trajectories with impact parameters in the range of 7–9 a.u. In Ne^{10+}-C_{60} collisions, the CBM predicts that the first to the tenth electrons are transferred to n levels ranging from $n=9$ to 4, in good agreement with the calculation of Langereis *et al.* [[12] (Fig. 6)]. In collisions through the electronic clouds, the impact parameter is shorter than R_{10} (12 a.u.) [11]; a large number of electrons are tranferred simultaneously and occupy the same inner *N* shell leading to the formation of the compact hollow atom of the first generation (CHA1). The measured ejected electron distribution provides insight into the fast Auger decay of such compact hollow atoms.

The Auger decay of hollow atoms with electron occupation on the same shell is considered under two assumptions. First, only $(n\ell, n\ell')$ electron pair Auger processes are taken into account. Auger decays involving three or more electrons are neglected. Second, the quantum jump $\Delta n=n-n'$ between the initial n and final n' states of the bound electron is equal to $\Delta n=1$. Vaeck *et al.* have shown that the $\Delta n=1$ transition channels are opened when the number of electrons on the same shell is large [27]. A completely neutralized CHA1 has 10 electrons on the $n=4$ level (*N* shell). The Auger decay of such a hollow atom takes place in several phases. In the first phase, five electrons are ejected via autoionization and five electrons jump on the $n=3$ level $(4\ell^{10}\rightarrow\varepsilon\ell^5,3\ell^5)$. In the second phase, two electrons are ejected and two electrons jump on the $n=2$ level $(3\ell^5\rightarrow\varepsilon\ell^2,2\ell^2,3\ell)$ and finally one electron is ejected and one jumps to the *K* shell $(2\ell^2,3\ell'\rightarrow\varepsilon\ell'',1s,3\ell)$. In total, we find that eight electrons could be ejected from a completely neutralized hollow atom with 10 active electrons on the $n=4$ shell. Let us take into account the fact that Auger decay occurs during the interaction time, and after the loss of each electron, the target supplies another electron to neutralize again the CHA1. Taking the assumption that the electrons transferred after the fast electron ejection occupy also the same level on the projectile $n=4$, we can estimate the maximum number of active electrons for events with $s=2$. In fact, to stabilize two electrons on the *K* shell by Auger electron-pair decay, we need four electrons on the *L* shell, eight electrons on the *M* shell, and 16 electrons on the *N* shell. Therefore, at maximum, 16 electrons can be transferred to the N shell during the interaction time, leading to the stabilization of two of them. Despite the roughness of the previous analysis, comparison with experimental results shows a relatively good agreement. Indeed, for s=2 IN collisions (Fig. 4), the maximum number of active electrons is found to be 17, close to the estimated value of 16. The average experimental value of active electrons ($\langle r \rangle \simeq 13$) can be explained by electron transfers on lower states ($n<4$) leading to a smaller number in autoionization cascades.

IV. CONCLUSION

We have measured the partial cross sections for multicapture processes in collisions of Ne^{10+} with C_{60}. Collision events have been separated roughly upon the impact parameters using the projectile energy-loss analysis. The relaxation of three types of hollow atoms—HA1, CHA1, and HA2—has been studied selectively. For HA1, the observed linear dependence of the mean number $\langle n \rangle$ of ejected electrons versus the number s of stabilized electrons has been well reproduced using a statistical model. For HA2, we have observed a saturation effect of the mean electron number $\langle n \rangle$ for larger *s* value. This can be explained by a direct electron capture on lower states of Ne^{10+} ions. Intermediate cases have been identified in collisions with scattered projectiles Ne^{8+} $(s=2)$ corresponding to the formation of CHA1 close to the C_{60} molecule. The maximum number of ejected electrons in these cases is interpreted by the fast quasicomplete autoionization cascades and continuous electron supply from the target to the hollow atom during the collisions.

ACKNOWLEDGMENTS

The experiments have been performed at the LIMBE (Ligne d'Ions Multichargés à Basse Energie) at GANIL in Caen. We are grateful to Laurent Manuoury and Jean-Yves Paquet for preparing high-quality ion beams and for their help during the run. This work has been supported by the Region Rhone Alpes under Grant No. 97027-223 of the Convention Recherche, Program Emergence.

[1] J. Burgdörfer, P. Lerner, and F. W. Meyer, Phys. Rev. A **A44**, 5674 (1991).
[2] H. Kurz, K. Töglhofer, H. P. Winter, and F. Aumayr, Phys. Rev. Lett. **69**, 1140 (1992).
[3] J. P. Briand, S. Thuriez, G. Giardino, G. Bursoni, M. Froment, M. Eddrief, and C. Sebenne, Phys. Rev. Lett. **77**, 1452 (1996).
[4] S. Winecki, C. L. Cocke, D. Fry, and M. P. Stöckli, Phys. Rev. A **53**, 4228 (1996).
[5] M. Grether, D. Niemann, A. Spieler, and N. Stolterfoht, Phys. Rev. A **56**, 3794 (1997).
[6] H. P. Winter and F. Aumayr, J. Phys. B **32**, R39 (1999).
[7] N. Stolterfoht, J. H. Bremer, and R. Diez Muino, Int. J. Mass. Spectrom. **192**, 425 (1999).
[8] S. Ninomiya, Y. Yamazaki, F. Koike, H. Masuda, T. Azuma, K. Komaki, K. Kuroki, and M. Sekiguchi, Phys. Rev. Lett. **78**, 4557 (1997).
[9] U. Thumm, Phys. Rev. A **55**, 479 (1997).
[10] Martin, L. Chen, A. Denis, and J. Désesquelles, Phys. Rev. A **57**, 4518 (1998).
[11] H. Cederquist, A. Fardi, K. Haghighat, A. Langereis, H. T. Schmidt, S. H. Schwartz, J. C. Levin, I. A. Sellin, H. Lebius, B. Huber, M. O. Larsson, and P. Hvelplund, Phys. Rev. A **61**, 022712 (2002).
[12] A. Langereis, J. Jensen, A. Fardi, K. Haghighat, H. T. Schmidt, S. H. Schwartz, H. Zettergren, and H. Cederquist, Phys. Rev. A **63**, 062725 (2001).
[13] J. P. Briand, L. de Billy, J. Jin, H. Khemliche, M. H. Prior, Z. Xie, M. Nectoux, and D. H. Schneider, Phys. Rev. A **53**, R2925 (1996).
[14] N. Vaeck and N. J. Kylstra, Phys. Rev. A **65**, 062502 (2002).
[15] S. Martin, R. Bredy, J. Bernard, J. Désesquelles, and L. Chen, Phys. Rev. Lett. **89**, 183401 (2002).
[16] M. Hattas, Schenkel, A. Hamza, A. V. Barnes, M. W. Newman, J. W. McDonald, T. R. Niedermayr, G. A. Machicoane, and D. H. Schneider, Phys. Rev. Lett. **82**, 4795 (1999).
[17] R. Brèdy, Ph.D. thesis, Université Claude Bernard Lyon I, France, 2001.
[18] L. Chen, J. Bernard, A. Denis, S. Martin, and J. Désesquelles Phys. Scr., T **80** 52 (1999).
[19] A. Russek and J. Meli, Physica (Amsterdam) **46**, 222 (1970).
[20] S. Martin, L. Chen, A. Denis, R. Bredy, J. Bernard, and J. Désesquelles, Phys. Rev. A **62**, 022707 (2000); J. Bernard, R. Bredy, S. Martin, L. Chen, J. Désesquelles, and M. C. *ibid.* **66**, 013209 (2002).
[21] J. F. Ziegler, *Handbook of Stopping Cross Sections for Energetic Ions in All Elements* (Pergamon, New York, 1985).
[22] T. Kunert and R. Schmidt, Phys. Rev. Lett. **86**, 5258 (2001).
[23] N. Bohr, K. Dan. K. Dan. Vidensk. Selsk. Mat. Fys. Medd. **18**, 8 (1989).
[24] S. Martin, R. Bredy, J. Bernard, L. Chen, M. C. Buchet-Poulizac, and A. Salmoun, Nucl. Instrum. Methods Phys. Res. B (to be published).
[25] R. Brèdy, L. Chen, S. Martin, J. Bernard, and J. Désesquelles, Phys. Scr., T **T92**, 141 (2001).
[26] J. Bernard, L. Chen, A. Salmoun, R. Bredy, and S. Martin, Phys. Rev. A (to be published).
[27] N. Vaeck and J. E. Hansen, J. Phys. B **28**, 3523 (1995).